

Cite this: *Nanoscale*, 2012, **4**, 3111

www.rsc.org/nanoscale

## Giant magnetoresistance in silicene nanoribbons†

Chengyong Xu,<sup>a</sup> Guangfu Luo,<sup>ab</sup> Qihang Liu,<sup>a</sup> Jiaxin Zheng,<sup>ac</sup> Zhimeng Zhang,<sup>a</sup> Shigeru Nagase,<sup>b</sup> Zhengxiang Gao<sup>a</sup> and Jing Lu<sup>\*a</sup>

Received 5th January 2012, Accepted 16th March 2012

DOI: 10.1039/c2nr00037g

By performing first-principle quantum transport calculations, we predict a giant magnetoresistance in zigzag silicene nanoribbons (ZSiNRs) connecting two semi-infinite silicene electrodes through switch of the edge spin direction of ZSiNRs. Spin-filter efficiency of both the antiferromagnetic and ferromagnetic ZSiNRs is sign-changeable with the bias voltage. Therefore, potential application of silicene in spintronics devices is suggested.

## 1. Introduction

Graphene, flat single-layer graphite with hexagonal structure, has aroused considerable research enthusiasm experimentally<sup>1,2</sup> and theoretically<sup>3,4</sup> ever since its first mechanical isolation.<sup>1</sup> Its unique properties, such as massless Dirac Fermion behavior,<sup>5,6</sup> high mobility,<sup>1,7</sup> long spin relaxation time and length,<sup>2,8,9</sup> and anomalous quantum Hall effect<sup>10,11</sup> make it a promising candidate for future electronic devices. Geometric confinement of the two-dimensional graphene sheet yields quasi one-dimensional graphene nanoribbons (GNRs).<sup>12,13</sup> The various properties of GNRs have been widely investigated<sup>14–16</sup> as well. The unique properties of graphene evoke interest in honeycomb single-layer structures formed by other group IV elements: Si, Ge, and Sn (referred to as silicene, germanene, and silybene, respectively).

Silicene has been fabricated experimentally by means of depositing silicon on Ag(111) surfaces.<sup>17</sup> First-principles calculations have predicted that the most stable structure of silicene and germanene has a buckling configuration.<sup>18</sup> The method of depositing silicon has been used to grow perfectly aligned silicene nanoribbons (SiNRs) on Ag(110)<sup>19</sup> or (100)<sup>20</sup> surfaces, and the nanoribbons are 16 Å in width and several hundred nanometers in length. Both STM<sup>19</sup> and density functional theory (DFT)<sup>21</sup> show that these nanoribbons are zigzag-edged with 5 chains across the width.

The band structure of silicene is similar to that of graphene and featured by a linearly-dispersed Dirac cone at the *K* points in the

Brillouin zone.<sup>18,22,23</sup> The ground state of a H-passivated zigzag SiNR (ZSiNR) has the two edges antiferromagnetically (AFM) coupled, which is slightly lower in energy than the state with the two edges ferromagnetically (FM) coupled. The AFM state of a ZSiNR is semiconducting, while the FM state is metallic. If applying a proper magnetic field, ZSiNRs can switch between the AFM and the FM configurations, and consequently a large magnetoresistance (MR) is expected because of a large current difference between the semiconducting AFM and the metallic FM configurations.<sup>24–27</sup> In a SiNR-based spintronics device, the spin-polarization of carriers will be partially kept when carriers have traveled across the conducting channel, as long as the channel length is shorter than the spin relaxation length.<sup>28</sup> One remarkable property of silicon-based spintronics devices is that charge carriers in silicon nanomaterials have very long spin relaxation times ( $\tau_s = 0.14$  ns for electrons and 0.27 ns for holes at 300 K (ref. 29)) and large spin coherence lengths ( $l_s = 0.23$  μm for electrons and 0.31 μm for holes at 300 K (ref. 29)), comparable to those in graphene ( $\tau_s = 0.1–0.4$  ns and  $l_s = 1.5–2.4$  μm at room temperature (ref. 9,30)). Another attractive property of silicon-based spintronics devices is their possible compatibility with the contemporary semiconductor industry.

In this article, we study the quantum transport properties of ZSiNRs connecting two semi-infinite silicene electrodes under finite bias voltages by using DFT coupled with non-equilibrium Green's function (NEGF) formalism. MR up to 1960% is predicted at 300 K, which is several times larger than the previous best experimental results at room temperature.<sup>31,32</sup> Moreover, the polarization direction of the current can be controlled by the bias voltage in both the AFM and FM configurations. To the best of our knowledge, this is the first theoretical work exploring the possible application of silicene in a spin-valve device.

## 2. Model and method

A supercell model is built to study silicene and ZSiNRs with the interlayer distance separated by 10 Å to eliminate possible mirror interaction. The edge silicon atoms of ZSiNRs are terminated

<sup>a</sup>State Key Laboratory of Mesoscopic Physics and Department of Physics, Peking University, Beijing 100871, P. R. China. E-mail: jinglu@pku.edu.cn

<sup>b</sup>Department of Theoretical and Computational Molecular Science, Institute for Molecular Science, Okazaki 444-8585, Japan

<sup>c</sup>Academy for Advanced Interdisciplinary Studies, Peking University, Beijing 100871, P. R. China

† Electronic supplementary information (ESI) available: The total current contrasts between the AFM and FM configurations and the spin-resolved  $I-V_{\text{bias}}$  characteristics in the AFM and FM configurations of all the checked ZSiNRs as a function of bias voltage; the spin-resolved  $I-V_{\text{bias}}$  characteristics and SFEs of different-length 5-ZSiNR in the AFM and FM configurations as a function of bias voltage. See DOI: 10.1039/c2nr00037g

with hydrogen atoms so as to eliminate the dangling bonds of silicon atoms.  $N$ -ZSiNR is used to denote a ZSiNR with  $N$  dimer chains across the ribbon width. In our study,  $N = 3, 4, 5, 6, 7$ , and  $8$  are considered. Geometry optimization and electronic structure calculations are performed with the double numerical plus polarization (DNP) basis set implemented in the DMol<sup>3</sup> package.<sup>33,34</sup> A generalized gradient approximation (GGA) of Perdew–Burke–Ernzerhof (PBE)<sup>35</sup> functional form is chosen to describe the exchange and correlation interaction. The positions of the atoms are relaxed until the maximum force on each atom is no more than  $0.01 \text{ eV } \text{Å}^{-1}$ . The first Brillouin zone is sampled with a  $6 \times 6 \times 1$ ,  $1 \times 6 \times 1$ ,  $50 \times 50 \times 1$ , and  $1 \times 50 \times 1$  Monkhorst–Pack<sup>36</sup>  $k$ -point mesh for optimization of silicene and ZSiNRs and energy band calculations of silicene and ZSiNRs, respectively.

Our junction consists of a finite ZSiNR connected to two semi-infinite silicene electrodes. This structure can be built by electron irradiating a protected silicene, like similar treatments based on graphene.<sup>37,38</sup> The AFM and FM configurations of two ZSiNRs are displayed in Fig. 1a and b, respectively. Two adjacent in-plane (out-of-plane) ZSiNRs are separated by no less than  $12.7$  ( $10$ ) Å to eliminate possible mirror interactions. All the finite ZSiNRs are  $44.0$  Å in length unless otherwise specified.

The relaxation and quantum transport calculation of our junctions are carried out by using DFT coupled with NEGF formalism implemented in the ATK package,<sup>39–41</sup> utilizing the GGA-PBE<sup>35</sup> form of functionals, single-zeta (SZ) basis set, and  $10 \times 1 \times 100$  Monkhorst–Pack<sup>36</sup>  $k$ -point mesh. Hellmann–Feynman forces after the relaxation are no more than  $0.05 \text{ eV } \text{Å}^{-1}$  on each atom. The temperature of electrodes is set to  $300 \text{ K}$ . At room-temperature, the mean free paths of electrons and phonons in bulk silicon are in order of micrometers.<sup>42,43</sup> The spin-coherence length of carriers in bulk silicon are  $l_s = 0.23 \text{ } \mu\text{m}$  for electrons and  $0.31 \text{ } \mu\text{m}$  for holes.<sup>29</sup> If the mean free paths and spin-coherence lengths of carriers in silicene and SiNRs are similar to those in bulk silicon, our SiNR-based devices ( $7.7$  or  $9.6 \text{ nm}$  in total length) would work well at room temperature.

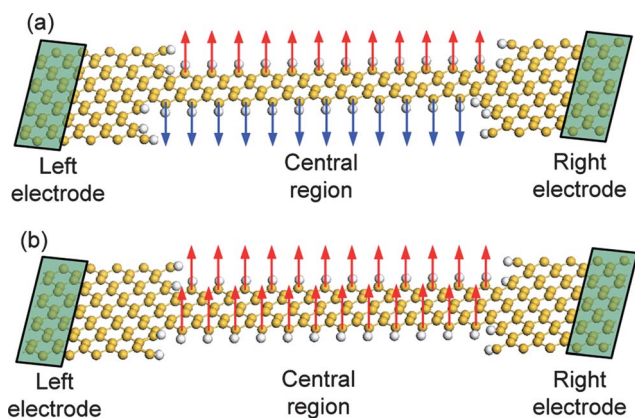


**Fig. 1** Schematic model of a H-passivated ZSiNR connected to two armchair-edged semi-infinite silicene structures. (a) The 3-ZSiNR in the AFM configuration. (b) The 4-ZSiNR in the FM configuration. Applying or removing magnetic field adjusts the ferromagnetic coupling of the two edges. The yellow (gray) balls denote silicon (hydrogen) atoms. The arrows represent spin directions on the edges.

Spin-polarized current under bias voltage is calculated using the Landauer–Buttiker formula:<sup>44</sup>

$$I_{\sigma}(V_{\text{bias}}) = \frac{e}{h} \int \left\{ T_{\sigma}(E, V_{\text{bias}}) \left[ f_{\text{L}}(E, V_{\text{bias}}) - f_{\text{R}}(E, V_{\text{bias}}) \right] \right\} dE, \quad (1)$$

where  $T_{\sigma}(E, V_{\text{bias}})$  is the spin-polarized transmission probability,  $f_{\text{L/R}}(E, V_{\text{bias}})$  is the Fermi–Dirac distribution function of the left (L)/right (R) electrode, and  $\sigma$  represents spin freedom.

Usually the optimistic definition is adopted to calculate MR, which is defined as:

$$\text{MR}(V_{\text{bias}}) = \frac{I_{\text{FM}} - I_{\text{AFM}}}{I_{\text{AFM}}}, \quad (2)$$

where  $V_{\text{bias}}$  is the applied bias voltage,  $I_{\text{FM}}$  ( $I_{\text{AFM}}$ ) is the total currents of the FM (AFM) configuration. Pessimistic definition of MR,  $(I_{\text{FM}} - I_{\text{AFM}})/I_{\text{FM}}$ , is not chosen because  $I_{\text{FM}}$  is generally much larger than  $I_{\text{AFM}}$  so that the pessimistic MR approaches close to 100%, which is hard to compare with each other.

Spin-filter efficiency (SFE) at a finite bias voltage is defined as

$$\text{SFE}(V_{\text{bias}}) = \frac{I_{\text{up}} - I_{\text{down}}}{I_{\text{up}} + I_{\text{down}}}, \quad (3)$$

where  $I_{\text{up}}$  ( $I_{\text{down}}$ ) is the current of up (down) spin.

### 3. Results and discussion

After relaxation, the silicene was found to have a hexagonal lattice constant of  $3.87 \text{ Å}$  and a buckling of  $0.45 \text{ Å}$ , consistent with earlier theoretical values.<sup>18</sup> Although the buckling of silicene suggests a  $\text{sp}^2$ – $\text{sp}^3$  hybridization in contrast to a pure  $\text{sp}^2$  hybridization in graphene, the band structure of silicene (Fig. 2a) are similar to that of graphene, featured by a Dirac cone near  $E_{\text{f}}$  at the highly symmetric  $K$  point.

When including the spin degeneracy, each edge of ZSiNRs is ferromagnetically coupled. The lowest energy state is the one

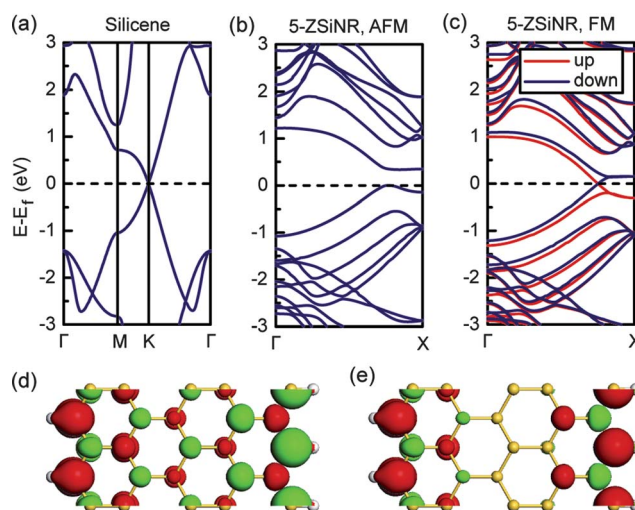


**Fig. 2** Band structures of (a) silicene, (b) the AFM 5-ZSiNR, and (c) the FM 5-ZSiNR. Spin density of (d) the AFM 5-ZSiNR and (e) FM 5-ZSiNR. The band structures of silicene and the AFM 5-ZSiNR are spin-degenerate but the FM 5-ZSiNR is non-degenerate. The isovalues of (d) and (e) are both  $0.004 \text{ a.u.}$

with antimagnetic coupling between the two edges, namely the AFM state, as illustrated by the spatial spin density distribution (Fig. 2d). With respect to the AFM state, a 5-ZSiNR is 7.8 meV per cell higher in the FM state, where the two edges are magnetically coupled as the spatial spin density shown in Fig. 2e. The nonmagnetic (NM) configuration of the 5-ZSiNR is 42.0 meV per cell higher than the AFM state.

In the AFM configuration, the magnetic ordering on the edges results in staggered sublattice potentials, realized by the opposite spin occupation on different sublattices,<sup>16</sup> especially on the opposite edges (Fig. 2d). The energy degeneracy of atoms on different sublattices no longer holds since the atoms experience different sublattice potentials, resulting in the separation of the conducting band and the valence band. Therefore, an energy gap is opened universally for the AFM ZSiNRs. In the FM configuration, however, there are no staggered sublattice potentials since the spin-up and spin-down occupation appears in both sublattices (Fig. 2e). Both the spin-up and spin-down electrons are free to propagate in the reciprocal space so that the FM state is metallic. From the band structures of the AFM and FM 5-ZSiNR, respectively plotted in Fig. 2b and c, we see clearly that the AFM case has a direct gap of 0.34 eV, while the FM case is metallic with two bands across  $E_f$ .

We utilize the difference between the semiconducting AFM and metallic FM states of a ZSiNR to obtain MR by using a magnetic field to switch the magnetic coupling between the two edges. When a magnetic field is absent, a ZSiNR stays at its semiconducting AFM ground state. The electronic transport is suppressed and occurs through tunneling. When a magnetic field is applied on the central ZSiNR, the ZSiNR is forced to enter the metallic FM state. The ballistic transport of electrons emerges throughout the conducting channel.

As shown in Fig. 3a, the currents of the finite FM 5-ZSiNR are obviously larger than those in the semiconducting AFM state. The currents of other ZSiNRs, provided in ESI,<sup>†</sup> exhibit similar behavior. Consequently, giant MRs (GMRs) for all the checked ZSiNRs are obtained, as displayed in Fig. 3b. The MRs of different ZSiNRs at the same bias voltage drop generally with increasing ribbon width, except 4-ZSiNR. In the examined bias range from 0.05 to 0.5 V, the MRs peak at  $V_{\text{bias}} = 0.05$  V for most ZSiNRs except the 4-ZSiNR (peaking at  $V_{\text{bias}} = 0.25$  V). The maximum MRs of the ZSiNRs are 261–1960%.

Traditionally, the most efficient MR junctions are those with insulating MgO layers bridging two ferromagnetic metals (FM/MgO/FM), and they are predicted to have a potential maximum optimistic MR of over 1000%.<sup>45–47</sup> In recent years, this limit has

been reached in CoFeB/MgO/CoFeB junctions with MR of 500–600% at 300 K<sup>31,32</sup> and 1100% at 5 K.<sup>31,32</sup> The rise of silicene as well as graphene provides possible alternative access to a new type of spin-valves with a larger MR than the FM/MgO/FM junctions. The maximum MRs of the checked ZSiNRs are comparable to or several times larger than the best experimental values at the room temperature.<sup>31,32</sup>

To provide an insight into the GMR behavior, we investigate the transmission spectrum, the spatially resolved local density of states (LDOS), and the spatially resolved transmission eigenstates of the 5-ZSiNR at  $V_{\text{bias}} = 0.2$  V. The transmission coefficients (Fig. 4a) of the FM configuration are always higher than those of the AFM case throughout the whole bias voltage window. Such a difference in the transmission spectra between the AFM and the FM configurations is in accord with the difference in the currents, according to eqn (1). The LDOS at  $E_f$  of the AFM (FM) configuration is shown in Fig. 4b and c. The LDOS decreases from both sides to the middle in the AFM configuration but remains almost invariant throughout the nanoribbon in the FM state. It is evident that the LDOS of the FM configuration is much higher than that of the AFM configuration in the middle of the ZSiNR. The difference between the AFM and FM configurations is also reflected in the spin-resolved transmission eigenstates, as presented in Fig. 4d–g. The transmission eigenstates of the spin-up (Fig. 4d) and spin-down (Fig. 4f) electrons in the AFM configuration are highly localized

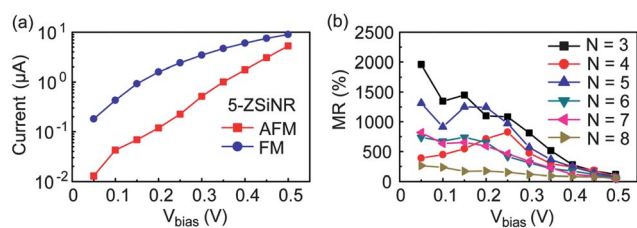


**Fig. 3** (a)  $I$ - $V_{\text{bias}}$  characteristics of the 5-ZSiNR at the AFM and FM configurations. (b) MRs of different-width ZSiNRs as a function of bias voltage.

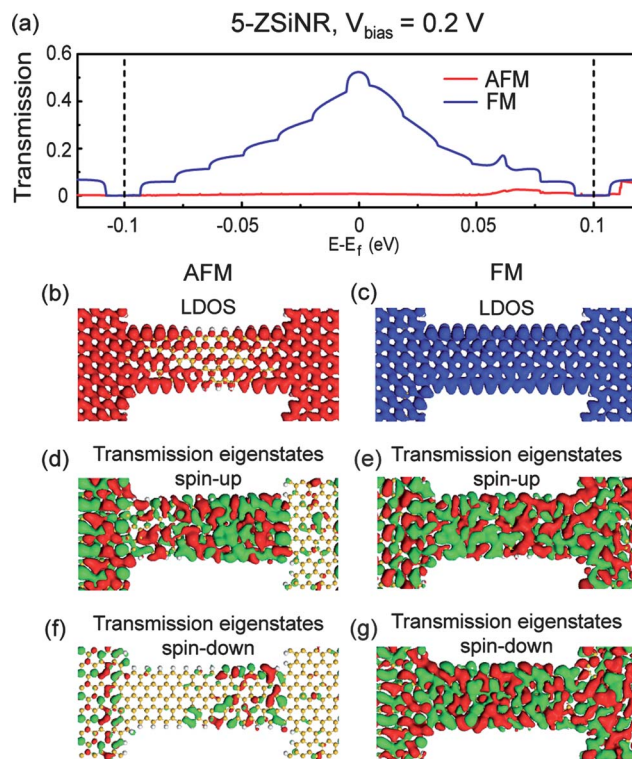


**Fig. 4** Transmission spectra, LDOSs, and transmission eigenstates of the AFM and FM 5-ZSiNR at  $V_{\text{bias}} = 0.2$  V. (a) Transmission spectra. Dashed lines denote the bias voltage window. (b) and (c) LDOSs at  $E_f$ . (d)–(g) Transmission eigenstates at  $E_f$  and the  $\Gamma$  point. The red (green) in (d)–(g) indicates the positive (negative) values of the wave functions. The isovalues of (d) and (c) are 0.001 a.u., and (d)–(g) are 0.01 a.u.

and nearly vanish at the right electrode area, resulting in a blockade of electron transport. In contrast, the transmission eigenstates of the FM configuration (Fig. 4e and g) are continuously distributed throughout the two-probe model, causing the metallic conduction. The contrasts in the transmission spectra, LDOSs, and transmission eigenstates converge to one point: that the currents in the FM configuration are much larger than those in the AFM configuration.

Our earlier quantum transport calculations predicted a maximum MR up to about 4000% at room temperature for a similar two-probe model based on a zigzag graphene nanoribbon (ZGNR) channel and graphene electrodes,<sup>26</sup> where the same transition mechanism works. The reason why the MRs of  $N$ -ZSiNRs are not as large as those of  $N$ -ZGNRs at the same bias voltage lies in the fact that an AFM ZSiNR has a smaller band gap than the AFM ZGNR with the same  $N$ . For example, the band gap of the AFM 5-ZSiNR (0.34 eV) is only 62% of that of the AFM 5-ZGNR (0.55 eV) obtained by the same DFT method. Therefore, the tunneling of electrons is less suppressed in the AFM  $N$ -ZSiNR than in the AFM  $N$ -ZGNR, resulting in the currents of the former being about one order of magnitude larger at the same bias voltage. On the other hand, the currents in the FM  $N$ -ZSiNR are only two to three times larger than the currents in the FM  $N$ -ZGNR at the same bias voltage. The combination of the contrasting effects mentioned above yields smaller MRs of the ZSiNRs than the ZGNRs with the same  $N$  at the same bias voltage.

Another type of spin-valve based on ZGNRs has been proposed,<sup>24</sup> where ZGNRs serve as the electrodes. It works by changing the relative magnetic directions on the opposite ZGNR electrodes. The predicted GMR is up to 1 million percent for H-passivated ZGNR devices<sup>24</sup> and 1 billion percent for bare ZGNR devices<sup>25</sup> at room temperature. This is because of the requirement of additional orbital symmetry matching in addition to the traditional spin matching. Experimentally, the current of GNRs (width  $\sim 15$  nm and length  $\sim 800$  nm) can be tuned by a magnetic field, with maximum optimistic MR around 130% at 285 K.<sup>37</sup> However, the mechanism of this MR is that a perpendicular magnetic field reduces the quantum confinement through the emergence of cyclotron orbits.<sup>48–50</sup>

The spin-resolved  $I$ - $V_{\text{bias}}$  characteristics of the 3-ZSiNR (6-ZSiNR) in the AFM and FM configurations are presented in Fig. 5a and b. The current with up spin of the FM 3-ZSiNR is larger than that with down spin as  $V_{\text{bias}} \leq 0.3$  V but smaller than the latter as  $V_{\text{bias}} > 0.3$  V. Therefore, the current polarization of the 3-ZSiNR can be controlled by the bias voltage. In contrast, the current with up spin of the FM 6-ZSiNR is always larger than that with down spin. The spin-resolved  $I$ - $V_{\text{bias}}$  characteristics of other ZSiNRs are provided in the ESI.† The SFEs of the six ZSiNRs are shown in Fig. 5c–f. The AFM asymmetric ZSiNRs ( $N = 3, 5,$  and  $7$ ) (Fig. 5c) have larger absolute maximum SFEs than the symmetric ones ( $N = 4, 6,$  and  $8$ ) (Fig. 5d). The absolute maximum SFEs are 19%, 9%, and 9% for the 3-, 5-, and 7-ZSiNR, respectively. The SFEs of the AFM symmetric ZSiNRs are no more than 3% and can almost be neglected. Sign-switching of SFEs are obtained in the AFM 3- and 5-ZSiNR. Such reversal of spin-polarization induced by bias voltage could find a potential use in logic spintronics devices. Actually, this reversal has already been detected experimentally in the Fe/GaAs

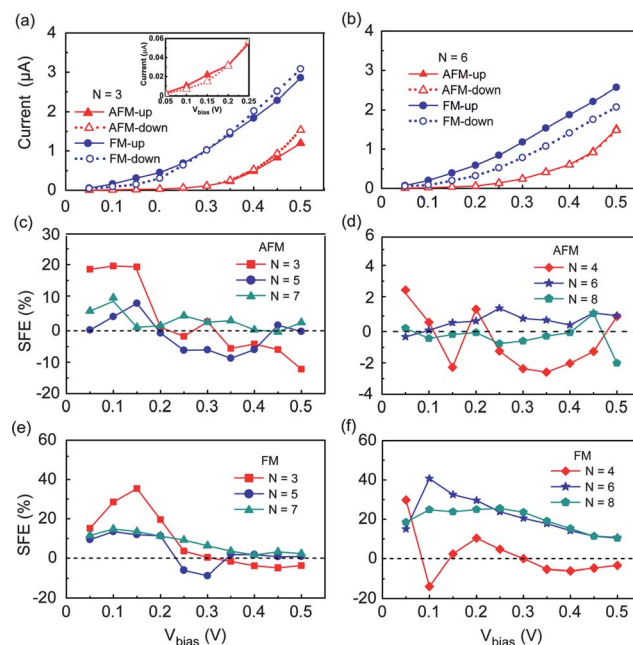


**Fig. 5** Spin-resolved  $I$ - $V_{\text{bias}}$  characteristics of (a) the 3-ZSiNR and (b) 6-ZSiNR in the AFM and FM configurations. SFE of the (c) AFM asymmetric, (d) AFM symmetric, (e) FM asymmetric, and (f) FM symmetric ZSiNRs as a function of bias voltage. Inset in panel (a): Spin-resolved  $I$ - $V_{\text{bias}}$  characteristics of the 3-ZSiNR under a bias voltage less than 0.25 V. The currents with up spin and down spin of the 6-ZSiNR in the AFM configuration nearly coincide in panel (b).

(001) interface<sup>8</sup> and predicted theoretically in the organic molecular junction.<sup>51</sup> Among the FM asymmetric ZSiNRs, the 3-ZSiNR apparently has a larger absolute maximum SFE than 5- and 7-ZSiNR (Fig. 5e). The absolute maximum SFEs of the FM 3-, 5-, and 7-ZSiNRs are 35%, 13%, and 15%, respectively. The absolute maximum values of SFEs of the FM 4-, 6-, and 8-ZSiNRs are 30%, 41%, and 26%, respectively. Notably, the FM 3-, 4-, and 5-ZSiNR also show sign-changing SFE against bias voltage.

To analyze the origin of the SFE, we study the transmission spectra, LDOSs at  $E_f$ , and transmission eigenstates at the  $E_f$  and  $\Gamma$  points of the AFM 3-ZSiNR at  $V_{\text{bias}} = 0.15$  V (the left column of Fig. 6), at  $V_{\text{bias}} = 0.5$  V (the middle column of Fig. 6), and the FM 6-ZSiNR at  $V_{\text{bias}} = 0.1$  V (the right column of Fig. 6). The transmission coefficients of spin up electron are larger than or equivalent to those of spin down electron within the bias voltage window for the AFM 3-ZSiNR at  $V_{\text{bias}} = 0.15$  V (Fig. 6a). The difference between the LDOSs of spin up and spin down electrons is not in the central region but in the electrode area. The LDOS of a spin up electron (Fig. 6d) is connected in the electrode area, while that of a spin down (Fig. 6g) electron is more localized and forms hexagonal rings. In the right electrode area, the transmission eigenstate of a spin down electron (Fig. 6m) is slightly more localized than the spin up case (Fig. 6j). The contrasts mentioned above all indicate that the spin up electron dominates over the spin down electron for AFM 3-ZSiNR, in agreement with a positive SFE (19%) at  $V_{\text{bias}} = 0.15$  V. However, the dominance between the spin up and spin down electrons of the AFM 3-ZSiNR is overturned at  $V_{\text{bias}} = 0.5$  V.

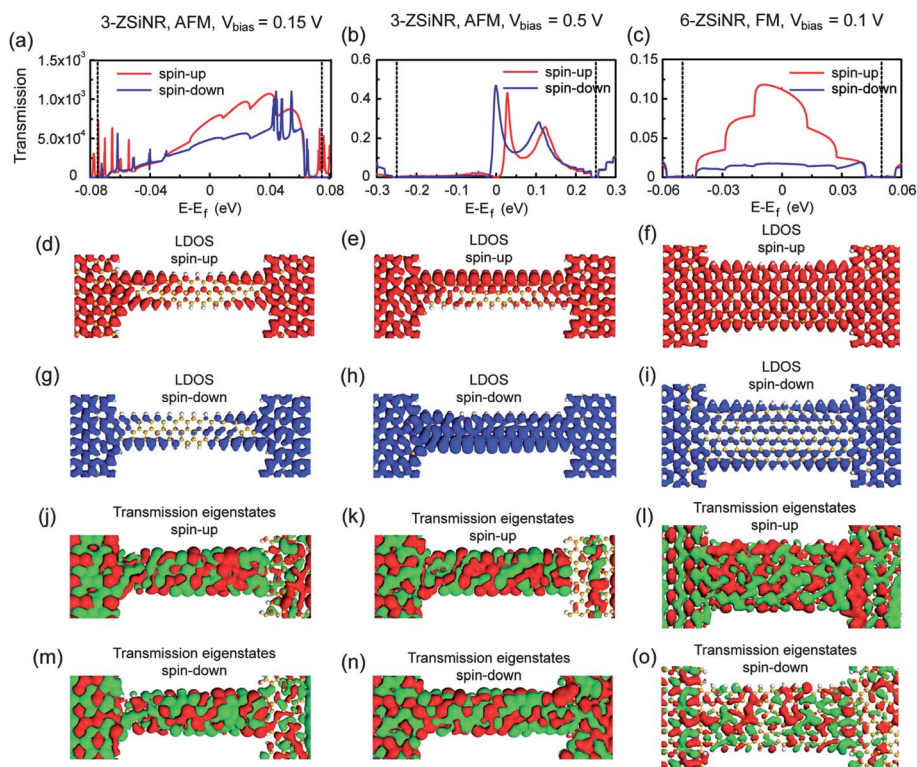


**Fig. 6** Transmission spectra, spin-resolved LDOSs, and spin-resolved transmission eigenstates of the AFM 3-ZSiNR at  $V_{\text{bias}} = 0.15$  V (left column), the AFM 3-ZSiNR at  $V_{\text{bias}} = 0.5$  V (middle column), and the FM 6-ZSiNR at  $V_{\text{bias}} = 0.1$  V (right column), respectively. (a)–(c) Transmission spectra, (d)–(i) LDOSs at  $E_f$ , (j)–(o) Transmission eigenstates at  $E_f$  and at the  $\Gamma$  point in the Brillouin zone. The red (green) in (j)–(o) indicates the positive (negative) values of the wave functions. The isovalues of (d)–(i) are 0.001 a.u., (j) and (m) are 0.002 a.u., (k) and (n) are 0.004 a.u., and (l) and (o) are 0.01 a.u.

The comparison of transmission spectra (Fig. 6b), LDOSs (Fig. 6e and h), and transmission eigenstates (Fig. 6k and n) all indicate a dominance of the spin down electron over the spin up electron for the AFM 3-ZSiNR at  $V_{\text{bias}} = 0.5$  V, in accord with a negative SFE of  $-12\%$ . The changing dominance of the two spins from  $V_{\text{bias}} = 0.15$  to  $0.5$  V explains the sign-changing of the SFEs in the AFM 3-ZSiNR. The contrasts of transmission spectra (Fig. 6c), LDOSs (Fig. 6f and i), and transmission eigenstates (Fig. 6l and o) in the FM 6-ZSiNR at  $V_{\text{bias}} = 0.1$  V suggest that the spin up electron dominates over the spin down electron and results in a positive SFE of  $41\%$ .

We then checked the dependence of the currents, GMR, and SFE on the length of ZSiNRs. The tunneling currents in the AFM ZSiNRs are reduced with the increasing ribbon length, while the metallic transport current in the FM ZSiNRs did not change significantly (Fig. 7a). Therefore, the MRs are generally enhanced as the ribbon length increases (Fig. 7b). The SFEs change insignificantly with increasing ribbon length. The spin-resolved currents and SFEs of the 5-ZSiNR in the AFM and FM configurations with different ribbon lengths are presented in the ESI†.

The magnetic moments of the two outmost edge Si atoms of the infinite 5-ZSiNR are  $0.34$  and  $-0.34 \mu_B$  in the AFM configuration, while both the magnetic moments are  $0.31 \mu_B$  in the FM configuration. These magnetic moments of the edge Si atoms are about one order of magnitude larger than those of the central Si atoms regardless of the spin coupling between the two edges. The critical magnetic field  $B^*$  required to switch a ZSiNR between the

AFM and FM configurations can be estimated from the relation:<sup>27</sup>

$$B^* = \frac{\Delta}{g\mu_B M_T}, \quad (4)$$

where  $\Delta$  is the energy difference between the AFM and FM configurations,  $g = 2$  is the Landauer factor of silicene,  $\mu_B = 0.058 \text{ meV T}^{-1}$  is the Bohr magneton, and  $M_T$  is the total spin on edge atoms. The resulting  $B^*$  of the 5-ZSiNR is  $8.6$  T, which is easily attainable in the laboratory.

So far the spin correlation length  $l_s$ , a physical quantity enabling the operation of a spin-valve, in a one-dimensional ZSiNR has not been investigated. We can simply estimate it according to the  $l_s$  of ZGNRs<sup>52</sup> because the spin states in both kinds of nanoribbons stem from the hybrid  $p_z$  orbitals at the

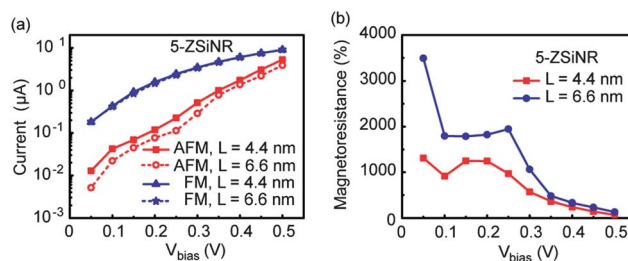


**Fig. 7** (a)  $I$ – $V_{\text{bias}}$  characteristics and (b) MRs of different-length 5-ZSiNR in the AFM and FM configurations.

zigzag edge atoms.<sup>14</sup> We notice that the spin diffusion lengths in silicon materials are also comparable to those in carbon materials.<sup>28</sup> The calculated 7.8 meV energy difference between the AFM and FM 5-ZSiNR corresponds to a temperature of 90.5 K, above which the AFM state can transit to the FM state spontaneously and the device is invalidated. At 90.5 K, the calculated  $l_s$  of a ZGNR edge is about 4–5 nm.<sup>52</sup> Thus we estimate the  $l_s$  of a ZSiNR edge to be about 4–5 nm at 90.5 K. The lengths of the ZSiNRs in our devices (4.4 or 6.6 nm) are in the same scale, suggesting that the devices work properly at 90.5 K. The spin correlation length grows inversely or exponentially with decreasing temperature,<sup>52</sup> and therefore the spintronics devices we proposed can operate more efficiently below 90.5 K.

Since the planar silicene and perfectly aligned ZSiNRs have been successfully fabricated, the device fabrication and property measurements become feasible. Direct measurement of spin relaxation time and coherence length of silicene and SiNRs are in urgent demand, as they will provide the fundamental basis for further research on silicene-based spin-valves.

#### 4. Conclusion

In summary, we have studied the electron transport properties of finite ZSiNRs connecting two planar silicene electrodes. We find that the devices, especially with narrow ZSiNRs, have a remarkable GMR at a finite bias voltage. The devices also have a sign-changeable SFE with respect to the bias voltage. Based on the giant magnetoresistance and sign-changeable spin-filter efficiency, our devices are potentially useful in nanoscale silicon spintronics.

#### Acknowledgements

This work was supported by National 973 Projects (No. 2007CB936200, MOST of China), the Program for New Century Excellent Talents in the University of MOE, the National Foundation for Fostering Talents of Basic Science (No. J0630311) of China, the Grant-in-Aid for Next Generation Super Computing Project (Nanoscience Program), and Specially Promoted Research from the MEXT in Japan.

#### References

- 1 K. S. Novoselov, A. K. Geim, S. V. Morozov, D. Jiang, Y. Zhang, S. V. Dubonos, I. V. Grigorieva and A. A. Firsov, *Science*, 2004, **306**, 666.
- 2 C. Berger, Z. M. Song, X. B. Li, X. S. Wu, N. Brown, C. Naud, D. Mayou, T. B. Li, J. Hass, A. N. Marchenkov, E. H. Conrad, P. N. First and W. A. de Heer, *Science*, 2006, **312**, 1191.
- 3 A. H. Castro Neto, F. Guinea, N. M. R. Peres, K. Novoselov and A. K. Geim, *Rev. Mod. Phys.*, 2009, **81**, 109.
- 4 D. S. L. Abergel, V. Apalkov, J. Berashevich, K. Ziegler and T. Chakraborty, *Adv. Phys.*, 2011, **59**, 261.
- 5 K. S. Novoselov, A. K. Geim, S. V. Morozov, D. Jiang, M. I. Katsnelson, I. V. Grigorieva, S. V. Dubonos and A. A. Firsov, *Nature*, 2005, **438**, 197.
- 6 S. Y. Zhou, G. H. Gwonen, J. Graf, A. V. Fedorov, C. D. Spataru, R. D. Diehl, Y. Kopelevich, D. H. Lee, S. G. Louie and A. Lanzara, *Nat. Phys.*, 2006, **2**, 595.
- 7 A. Lherbier, X. Blase, Y. M. Niquet, F. Triozon and S. Roche, *Phys. Rev. Lett.*, 2008, **101**, 036808.
- 8 S. A. Crooker, M. Furis, X. Lou, C. Adelmann, D. L. Smith, C. J. Palmstrom and P. A. Crowell, *Science*, 2005, **309**, 2191.
- 9 N. Tombros, C. Jozsa, M. Popinciuc, H. T. Jonkman and B. J. van Wees, *Nature*, 2007, **448**, 571.
- 10 K. S. Novoselov, Z. Jiang, Y. Zhang, S. V. Morozov, H. L. Stormer, U. Zeitler, J. C. Maan, G. S. Boebinger, P. Kim and A. K. Geim, *Science*, 2007, **315**, 1379.
- 11 Y. B. Zhang, Y. W. Tan, H. L. Stormer and P. Kim, *Nature*, 2005, **438**, 201.
- 12 J. Campos-Delgado, J. M. Romo-Herrera, X. T. Jia, A. DavidCullen, H. Muramatsu, Y. A. Kim, T. Hayashi, Z. Ren, D. J. Smith, Y. Okuno, T. Ohba, H. Kanoh, K. Kaneko, E. Endo, H. Terrones, M. S. Dresselhaus and M. Terrones, *Nano Lett.*, 2008, **8**, 2773.
- 13 X. L. Li, X. R. Wang, L. Zhang, S. Lee and H. J. Dai, *Science*, 2008, **319**, 1229.
- 14 M. Fujita, K. Wakabayashi, K. Nakada and K. Kusakabe, *J. Phys. Soc. Jpn.*, 1996, **65**, 1920.
- 15 Y. W. Son, M. L. Cohen and S. G. Louie, *Nature*, 2006, **444**, 347.
- 16 Y. W. Son, M. L. Cohen and S. G. Louie, *Phys. Rev. Lett.*, 2006, **97**, 216803.
- 17 L. Boubekeur, O. Hamid, E. Hanna, K. Abdelkader, V. Sebastien, E. Benidicte and A. Bernard, *Appl. Phys. Lett.*, 2010, **97**, 223109.
- 18 S. Cahangirov, M. Topsakal, E. Akturk, H. Sahin and S. Ciraci, *Phys. Rev. Lett.*, 2009, **102**, 236804.
- 19 C. Leandri, G. Le Lay, B. Aufray, C. Girardeaux, J. Avila, M. E. Davila, M. C. Asensio, C. Ottaviani and A. Cricenti, *Surf. Sci.*, 2005, **574**, L9.
- 20 Y.-L. Song, Y. Zhang, J.-M. Zhang and D.-B. Lu, *Appl. Surf. Sci.*, 2010, **256**, 6313.
- 21 A. Kara, S. Vizzini, C. Leandri, B. Ealet, H. Oughaddou, B. Aufray and G. Le Lay, *J. Phys.: Condens. Matter*, 2010, **22**, 045004.
- 22 G. G. Guzman-Verri and L. C. Lew Yan Voon, *Phys. Rev. B: Condens. Matter Mater. Phys.*, 2007, **76**, 075131.
- 23 Z. Ni, Q. Liu, K. Tang, J. Zheng, J. Zhou, R. Qin, Z. Gao, D. Yu and J. Lu, *Nano Lett.*, 2012, **12**, 113.
- 24 W. Y. Kim and K. S. Kim, *Nat. Nanotechnol.*, 2008, **3**, 408.
- 25 R. Qin, J. Lu, L. Lai, J. Zhou, H. Li, Q. H. Liu, G. F. Luo, L. N. Zhao, Z. X. Gao, W. N. Mei and G. P. Li, *Phys. Rev. B: Condens. Matter Mater. Phys.*, 2010, **81**, 233403.
- 26 C. Y. Xu, L. Z. Li, H. Li, R. Qin, J. X. Zheng, G. F. Luo, Q. H. Liu, X. Yan, L. L. Yu, J. Lu and Z. X. Gao, *Comput. Mater. Sci.*, 2011, **50**, 2886.
- 27 F. Munoz-Rojas, J. Fernandez-Rossier and J. J. Palacios, *Phys. Rev. Lett.*, 2009, **102**, 136810.
- 28 S. Sanvito, *Chem. Soc. Rev.*, 2011, **40**, 3336.
- 29 S. P. Dash, S. Sharma, R. S. Patel, M. P. de Jong and R. Jansen, *Nature*, 2009, **462**, 491.
- 30 W. Han and R. K. Kawakami, *Phys. Rev. Lett.*, 2011, **107**, 047207.
- 31 S. Ikeda, J. Hayakawa, Y. Ashizawa, Y. M. Lee, K. Miura, H. Hasegawa, M. Tsunoda, F. Matsukura and H. Ohno, *Appl. Phys. Lett.*, 2008, **93**, 082508.
- 32 Y. M. Lee, J. Hayakawa, S. Ikeda, F. Matsukura and H. Ohno, *Appl. Phys. Lett.*, 2007, **90**, 212507.
- 33 B. Delley, *J. Chem. Phys.*, 1990, **92**, 508.
- 34 B. Delley, *J. Chem. Phys.*, 2000, **113**, 7756.
- 35 J. P. Perdew, J. A. Chevary, S. H. Vosko, K. A. Jackson, M. R. Pederson, D. J. Singh and C. Fiolhais, *Phys. Rev. B: Condens. Matter*, 1992, **46**, 6671.
- 36 H. J. Monkhorst and J. D. Pack, *Phys. Rev. B: Solid State*, 1976, **13**, 5188.
- 37 J. W. Bai, R. Cheng, F. X. Xiu, L. Liao, M. S. Wang, A. Shailos, K. L. Wang, Y. Huang and X. F. Duan, *Nat. Nanotechnol.*, 2010, **5**, 655.
- 38 C. H. Jin, H. P. Lan, L. M. Peng, K. Suenaga and S. Iijima, *Phys. Rev. Lett.*, 2009, **102**, 205501.
- 39 *ATOMISTIX Toolkit version 2008.02*, QuantumWise A/S, www.quantumwise.com.
- 40 J. Taylor, H. Guo and J. Wang, *Phys. Rev. B: Condens. Matter Mater. Phys.*, 2001, **63**, 245407.
- 41 M. Brandbyge, J. L. Mozos, P. Ordejon, J. Taylor and K. Stokbro, *Phys. Rev. B: Condens. Matter Mater. Phys.*, 2002, **65**, 165401.
- 42 R. Gereth and K. Hubner, *Phys. Rev.*, 1964, **134**, A235.
- 43 L. Weber and E. Gmelin, *Appl. Phys. A: Solids Surf.*, 1991, **53**, 136.
- 44 S. Datta, *Electronic Transport in Mesoscopic Systems*, Cambridge University Press, Cambridge, 1995.

- 
- 45 W. H. Butler, X. G. Zhang, T. C. Schulthess and J. M. MacLaren, *Phys. Rev. B: Condens. Matter*, 2001, **63**, 054416.
- 46 J. Mathon and A. Umerski, *Phys. Rev. B: Condens. Matter*, 2001, **63**, 220403(R).
- 47 X. G. Zhang and W. H. Butler, *Phys. Rev. B: Condens. Matter Mater. Phys.*, 2004, **70**, 172407.
- 48 N. M. R. Peres, A. H. Castro Neto and F. Guinea, *Phys. Rev. B: Condens. Matter Mater. Phys.*, 2006, **73**, 195411.
- 49 N. M. R. Peres, A. H. Castro Neto and F. Guinea, *Phys. Rev. B: Condens. Matter Mater. Phys.*, 2006, **73**, 241403(R).
- 50 J. Zhu, S. Wei, N. Haldolaarachchige, J. He, D. P. Young and Z. Guo, *Nanoscale*, 2012, **4**, 152.
- 51 L. Wang, X. F. Gao, X. Yan, J. Zhou, J. Lu, Z. X. Gao, S. Nagase, S. Sanvito, Y. Maeda, T. Akasaka, W. N. Mei and J. Lu, *J. Phys. Chem. C*, 2010, **114**, 21893.
- 52 O. V. Yazyev and M. I. Katsnelson, *Phys. Rev. Lett.*, 2008, **100**, 047209.